Biogeosciences Discuss., 12, 17595–17641, 2015
www.biogeosciences-discuss.net/12/17595/2015/
doi:10.5194/bgd-12-17595-2015

Biogeosciences Discussions
Open Access

Estimates of common ragweed pollen emission and dispersion over Europe using RegCM-pollen model

L. Liu[1,2], **F. Solmon**[1], **R. Vautard**[3], **L. Hamaoui-Laguel**[3], **Cs. Zs. Torma**[1], and **F. Giorgi**[1]

[1]Earth System Physics Section, the Abdus Salam International Centre for Theoretical Physic, Trieste, Italy
[2]Guizhou Key Laboratory of Mountainous Climate and Resources, Guiyang, China
[3]National Center for Scientific Research, Paris, France

Received: 27 August 2015 – Accepted: 12 October 2015 – Published: 3 November 2015

Correspondence to: L. Liu (liliuliulish@outlook.com)

Published by Copernicus Publications on behalf of the European Geosciences Union.

Abstract

Common ragweed (*Ambrosia artemisiifolia* L.) is a highly allergenic and invasive plant in Europe. Its pollen can be transported over large distances and has been recognized as a significant cause of hayfever and asthma (D'Amato et al., 2007; Burbach et al., 2009). To simulate production and dispersion of common ragweed pollen, we implement a pollen emission and transport module in the Regional Climate Model (RegCM) version 4 using the framework of the Community Land Model (CLM) version 4.5. In the online model environment where climate is integrated with dispersion and vegetation production, pollen emissions are calculated based on the modelling of plant distribution, pollen production, species-specific phenology, flowering probability, and flux response to meteorological conditions. A pollen tracer model is used to describe pollen advective transport, turbulent mixing, dry and wet deposition.

The model is then applied and evaluated on a European domain for the period 2000–2010. To reduce the large uncertainties notably due to ragweed density distribution on pollen emission, a calibration based on airborne pollen observations is used. Resulting simulations show that the model captures the gross features of the pollen concentrations found in Europe, and reproduce reasonably both the spatial and temporal patterns of flowering season and associated pollen concentrations measured over Europe. The model can explain 68.6, 39.2, and 34.3 % of the observed variance in starting, central, and ending dates of the pollen season with associated root mean square error (RMSE) equal to 4.7, 3.9, and 7.0 days, respectively. The correlation between simulated and observed daily concentrations time series reaches 0.69. Statistical scores show that the model performs better over the central Europe source region where pollen loads are larger.

From these simulations health risks associated common ragweed pollen spread are then evaluated through calculation of exposure time above health-relevant threshold levels. The total risk area with concentration above 5 grains m^{-3} takes up 29.5 % of

domain. The longest exposure time occurs on Pannonian Plain, where the number of days per year with the daily concentration above 20 grains m^{-3} exceeds 30.

1 Introduction

Ambrosia artemisiifolia L. (common ragweed, hereafter ragweed), is an alien plant that has invaded parts of Europe over the last century, creating severe allergies in populations (Chauvel et al., 2006; Kazinczi et al., 2008; Gallinza et al., 2010; Pinke et al., 2011). It has been shown that concentrations of ragweed pollen down to 5–10 grains m^{-3} can lead to health problems for sensitive persons (Taramarcaz et al., 2005). In Europe, ragweed typically flowers from July to October (Kazinczi et al., 2008). Ragweed has developed wind pollination strategy, which allows each plant to produce millions of pollen grains with diameter of 18–22 µm and containing small air chambers (Payne, 1963). Pollen grains can readily become airborne when conditions are favourable (Dahl et al., 1999; Taramarcaz et al., 2005; Cecchi et al., 2006; Stach et al., 2007; Smith et al., 2008; Šikoparija et al., 2013).

One of the goals of the project "Atopic diseases in changing climate, land use and air quality" (http://www.atopica.eu) is to better understand and quantify the effects of environmental changes on ragweed pollen and associated health impacts over Europe. In this context the present study introduce a modelling framework designed to simulate production and dispersion of ragweed pollen. Ultimately these models can be used for investigating the effects of changing climate and land use on ragweed (Hamaoui-Laguel et al., 2015) and for providing relevant data to health impact investigators.

Presently a number of regional models, mostly designed for air quality prevision, incorporate release and dispersion dynamics of pollen (Helbig et al., 2004; Sofiev et al., 2006, 2013; Skjøth, 2009; Efstathiou et al., 2011; Zink et al., 2012; Prank et al., 2013; Zhang et al., 2014). Methods for producing ragweed pollen emission suitable for input to regional scale models have been developed in recent studies (Skjøth et al., 2010; Šikoparija et al., 2012; Chapman et al., 2014). Due to lack of statistical information related to plant location and amount within a given geographical area, the bottom up approach to produce plant presence inventories is unpractical for most herbaceous allergenic species like ragweed. Quantitative habitat maps for such species are often derived from spatial variations in annual pollen sum, knowledge on plant ecology and detailed land cover information by top-down approach (such as Skjøth et at., 2010, 2013). Lately, an observation-based habitat map of ragweed has been published in the context of the ENV.B2/ETU/2010/0037 project "Assessing and controlling the spread and the effects of common ragweed in Europe" (Bullock et al., 2012). This inventory is further calibrated against airborne pollen observations to reproduce the ragweed distribution with a high accuracy, according to Prank et al. (2013). Recently Hamaoui-Laguel et al. (2015) used the observations collected in Bullock et al. (2012), combined with simplified assumptions on plant density and a calibration using observations to obtain a ragweed density inventory map, which combined with a vegetation model (ORCHIDEE) and a phenology model (PMP) allowed to obtain daily available pollens (potential emissions) in Europe. Here we present a new approach with explicit treatment of pollen ripening, release and dispersion due to environmental driver in a fully online model environment where climate is integrated with dispersion and vegetation production.

On average, one ragweed plant can produce 1.19±0.14 billion pollen grains in a year (Fumanal et al., 2007), but resources available (solar radiation, water, CO_2, and nutrients) for individual during the growth season could alter plant fitness and further influence its pollen production (Rogers et al., 2006; Simard and Benoit, 2011, 2012). Fumanal et al. (2007) investigate the individual pollen production of different common ragweed populations in natural environment and propose a quantitative relationship between annual pollen production and plant biomass at the beginning of flowering. This allows to integrate the response of productivity to various environmental conditions through land surface model.

The timing of the emission can be estimated from a combination of phenological models and the species specific pollen release pattern driven by short-term meteorological conditions (Martin et al., 2010; Smith et al., 2013; Zink et al., 2013). Ragweed is a summer annual, short-day plant. Before seeds are able to germinate, it requires a period of chilling to break the dormant state (Willemsen, 1975). The following growth and phenological development depends on both temperature and photoperiod (Allard, 1945; Deen et al., 1998a). Flowering is initiated by a shortening length of day but could be terminated by frost (Dahl et al., 1999; Smith et al., 2013) or drought (Storkey et al., 2014). A number of phenological models have been developed for ragweed, either based on correlation fitting between climate and phenological stages (García-Mozo et al., 2009) or explicitly represented by biological mechanisms (Deen et al., 1998a; Shrestha et al., 1999; Storkey et al., 2014; Chapman et al., 2014). The mechanistic models take into account the responses of development rates to temperature, photoperiod, soil moisture, or stress condition (frost, drought, etc.). Mostly they are based on growth experiments but have to enforce a standard calendar date or a fixed day length for the onset of flowering when they are used in real condition. While the airborne pollen observations from European pollen monitoring sites have a high year to year, site to site variability. Therefore it might be practical to combine the mechanistic model with correlation fitting when the knowledge of plant physiology and local adaptation of phenology are not sufficiently known at the moment.

In this paper, we present a pollen emission scheme that incorporate plant distribution, pollen production, species-specific phenology, flowering probability distribution, and pollen release pattern based on recent studies findings. By combining the emission scheme with a transport mechanism a pollen simulation framework within the Regional Climate Model (RegCM) version 4 is then developed to study ragweed pollen dispersion behaviours on regional scale. In Sect. 2 we provide a description of the RegCM-pollen simulation configuration, emission parameterization details, the processing of plant spatial density and observations data used for calibration in the study. In Sect. 3 we define the model experiment, explain the method used to calibrate ragweed density, present the simulation results of pollen season and evaluate the performances of the coupled model system over a recent period covered with observations. The climatolog-

Discussion Paper | Discussion Paper | Discussion Paper | Discussion Paper |

BGD

12, 17595–17641, 2015

Estimates of common ragweed pollen emission and dispersion

L. Liu et al.

ical information about the ragweed pollen risk over European domain on decade-time scale is presented in Sect. 4.

2 Materials and methods

The development of RegCM-pollen model is based on the Abdus Salam International Centre for Theoretical Physics (ICTP) regional climate model, i.e. RegCM4, which has been used for a number of years in a wide variety of applications (Giorgi et al., 2006, 2012; Meleux et al., 2007; Pal et al., 2007). In this framework, we develop a pollen model for ragweed which calculates (i) the seasonal production of pollen grains and (ii) their emission and atmospheric processes (transport and deposition) determining regional pollen concentrations. As detailed hereafter pollen emission and transport are developed in the preexisting framework of the RegCM atmospheric chemistry module (Solmon et al., 2006, 2012; Zakey et al., 2006; Tummon et al., 2010; Shalaby et al., 2012). Pollen production is developed in the framework of the Community Land Model (CLM) version 4.5 (Oleson et al., 2013), which is the land surface scheme coupled to RegCM. Figure 1 gives an overview of such development framework. In the following subsections, we give details about the important data and steps of the development.

2.1 Observed pollen concentrations

Pollen observations are central for calibration and validation of the pollen module as discussed further. The pollen data are provided by the European Aeroallergen Network and affiliated national aerobiology monitoring network RNSA(France), ARPA-Veneto and ARPA-FVG(Italy), and Croatian monitoring sites. The archives cover ragweed pollen concentrations with daily resolution from 46 observations stations from 2000 to 2012 year (Fig. 2). The pollen observation sites range from 42.535 to 48.249° N and from 0.002 to 21.693° E. The sites are grouped for study purposes into four regions: France (FR), Italy (IT), Germany-Switzerland (DE + CH) and central Europe (Central

BGD
12, 17595–17641, 2015

EU) including Austria, Croatia, and Hungary. In most situations, ragweed pollens are collected using volumetric spore traps based on the Hirst (1952) design and counted under light microscopy (Jato et al., 2006; Skjøth et al., 2010; Zink et al., 2013; García-Mozo et al., 2009). We based our study on daily pollen concentrations, although for some stations hourly data are available. The observations period ranges from 2000 to 2012 but for some stations observations only cover part of this period.

2.2 Model setup

Ragweed pollen simulations are carried out for a European domain ranging from approximately 35 to 70° N, and from 20° W to 40° E (Fig. 2). The horizontal resolution is 50 km, with 23 atmospheric layers from the surface to 50 hPa. Initial and lateral atmospheric boundary conditions are provided by ERA-Interim analysis at 1.5° spatial resolution and 6 h temporal resolution. Weekly SSTs are obtained from the NOAA optimum interpolation (OI) SST analysis (with weekly ERA sea surface temperatures). Beside CLM4.5 as a land surface scheme, other important physical options are Holtslag PBL scheme (Holtslag et al., 1990) for boundary layer, Grell scheme (Grell, 1993) over land and Emanuel scheme (Emanuel and Zivkovic-Rothman, 1999) over ocean for convective precipitation, the SUBEX scheme (Pal et al., 2000) for large-scale precipitation. Aerosol and humidity are advected using a semi-Lagrangian scheme. The period 2000–2010 is chosen for the study. Even though the focus of the study is July–October of the flowering season, the model is integrated continuously throughout the year notably for simulating ragweed phenology. To compare with the observation described in Sect. 2.1, simulated pollen concentrations time series are interpolated to the station locations and averaged daily.

2.3 Ragweed spatial density

Ragweed spatial distribution is obtained through a procedure discussed in Hamaoui-Laguel et al. (2015) (Supplement). For country where observations are available and

BGD
12, 17595–17641, 2015

of sufficient quality, ragweed distribution is assumed to result from habitat suitability combined with infestation (not all suitable habitats are populated). The habitat suitability is assumed to scale as the product of the fraction of suitable land use surface $H(x,y)$ with a climate suitability index $\mathrm{CI}(x,y)$ calculated from the SIRIUS ecological model (Storkey et al., 2014). The infestation rate is derived from the density of 10 km × 10 km cells $K(x,y)$ with plant presence as reported in Bullock et al. (2012). Assuming a homogeneous surface distribution of suitable habitats within each model grid cell (50 km × 50 km) and assuming that observers only investigate suitable areas, the probability of plant presence (or infestation rate) should then be proportional to $K(x,y)/25$. But considering that an observer probably finds ragweed plants more often than what a random search would predict, the density should actually be lower than that predicted by $K(x,y)/25$. We assumed that infestation rate actually scales as $(K(x,y)/25)^r$, with $r > 1$, taken here equals to 2. The final ragweed density D_p (in plant m^{-2}) at 50 km resolution is therefore obtained from the infestation rate, surface fraction of suitable land use, and climatic suitability index as:

$$D_\mathrm{p}(x,y) = \mathrm{Const} \cdot H(x,y) \cdot \mathrm{CI}(x,y) \cdot \left(\frac{K(x,y)}{25}\right)^r \quad (1)$$

Here Const = 0.02 is assumed to be the maximal density (plant m^{-2}) in the most suitable habitats (Efstathiou et al., 2011), $H(x,y)$ taken as the crop and urban lands in CMIP5 land use classification (Hurtt et al., 2006). For countries with low-quality observations or with no available inventories, the detection probability is replaced by the average over neighbouring countries with reliable data.

2.4 Parameterization of the pollen emission flux

Pollen emission patterns on regional scale depend on plant density, production, and meteorological conditions. The parameterization of pollen emission flux is a modified version of Helbig et al. (2004). The vertical flux of pollen particles F_p in a given grid cell

BGD
12, 17595–17641, 2015

is assumed to be proportional to the product of a characteristic pollen grain concentration per plant individual c^* (grain m^{-3} plant^{-1}) and the local friction velocity u_*. This potential flux is then modulated by a plant-specific factor c_e that describes the likelihood of blossoming, and a meteorological adjustment factor. Finally the flux is scaled up at the grid level using the plant density D_p (plant m^{-2}) discussed previously in Sect. 2.2.

$$F_\mathrm{p} = D_\mathrm{p} \cdot c_e \cdot K_e \cdot c^* \cdot u_*. \tag{2}$$

2.5 Pollen production

The characteristic concentration c^* is related to pollen grain production using

$$c^* = \frac{q_\mathrm{p}}{\mathrm{LAI} \cdot H_\mathrm{s}} \tag{3}$$

where q_p is the annual pollen production in grains per individual plant (grains plant^{-1}), LAI = 3 is the leaf area index term, and $H_\mathrm{s} = 1$ is the canopy height (m). These later parameter are determined on the basis of C3 grass land use categories during summer.

Annual pollen production q_p is estimated from plant biomass production, based on an assumption that pollen production per plant is a function of the plant dry biomass i.e. the accumulated net primary production (NPP) of C3 grass CLM4.5 plant functional type during the growth season. Through this assumption, q_p is calculated following Fumanal et al. (2007) (Eq. 4). This parameterisation integrates the response of pollen grain productivity to various environmental conditions affecting C3 grass NPP, including climate variables and atmospheric CO_2 concentration for example. It involves a variety of biophysical and biogeochemical processes at the surface such as photosynthesis, phenology, allocation of carbon/nitrogen assimilates in the different components of plant, biomass turnover, litter decomposition, and soil carbon/nitrogen dynamics.

$$\mathrm{Log}_{10}(q_\mathrm{p}) = 7.22 + 1.12 \log_{10}(\text{plant dry biomass}) \tag{4}$$

In this approach, yearly total pollen production calculation from mature plant dry biomass needs to be determined in advance, i.e. before integration of the pollen modelling chain. This is done by making a preliminary RegCM-CLM4.5 run with prognostic NPP activated and archived. Alternatively, in order to reduce simulation costs and insure model portability to other domain we also built a precomputed global C3 grass yearly accumulated NPP data base. This data can be directly interpolated and prescribed to RegCM4 for pollen runs. This global data base is built by running the land component CLM45 of the Community Earth System Model version 1.2 (CESM1.2) (Oleson et al., 2013) with the Biome-BGC biogeochemical model (Thornton et al., 2002, 2007) enabled and forced by CRUNCEP (Viovy, 2011). We acknowledge that NPP obtained this way is not fully consistent with RegCM simulated climate but this approach represents a reasonable and practical compromise.

2.6 Flowering probability density distribution

In Eq. (2), C_e is a probability density function accounting for the likelihood of the plant to flower and effectively release pollen in the atmosphere. The inflorescences of common ragweed consist of many individual flowers that reach anthesis sequentially (Payne, 1963). At the beginning of the season only a few plants flower and the amount of available pollen grains is small, regardless of the favourable meteorological conditions. The number of flowers increases with time until a maximum is reached. Afterwards, the number decreases again until the end of the pollen season. To represent this dynamic, we use the normal distribution function reported in Prank et al. (2013). The probability distribution of flowering time is represented by Gaussian depending on “accumulated biological days” BD, and centred midway between flowering starting and ending biological days BD_{fe} and BD_{fs}:

$$c_e = \text{const} \cdot \frac{1}{\sigma\sqrt{2\pi}} \cdot e^{-\frac{\left(BD - \frac{BD_{fe}+BD_{fs}}{2}\right)^2}{2\sigma^2}} \tag{5}$$

BGD
12, 17595–17641, 2015

where const = 20×10^{-4} is determined by adjusting the integrated amount of pollens between BD_{fe} and BD_{fs} to the total yearly production q_p determined from NPP. σ is standard deviation determined by the length of the season, considering that the season represents about four standard deviations Gaussian distribution $4\sigma = BD_{fe} - BD_{fs}$. The probability distribution is however set to zero as soon as daily minimum temperature is below 0°, considering that first frost set up the end of ragweed activity (Dahl et al., 1999). In the following section we describe how biological days (BD) are effectively determined.

2.7 Phenology representation and flowering season definition

2.7.1 Biological days

For simulating the timing of the flowering season, we adapt the mechanistic phenology model of Chapman et al. (2014), which is based on growth experiments (Deen et al., 1998a, b, 2001; Shrestha et al., 1999). Phenology is simulated using BD accumulated for the current year of simulation and from the first day (t_0) after the spring equinox for which daily minimum temperature exceeds a certain threshold T_{min} defined further (Chapman et al., 2014). BD on time t depends on key environmental variables through:

$$\mathrm{BD}(T, L, \theta) = \int_{t_0} r_T(T) \cdot r_L(L) \cdot r_S(\theta) \cdot \mathrm{d}t \quad (6)$$

where r_T, r_L, r_S are the response of development rates to temperature T, photoperiod L, and soil moisture θ, respectively. In this approach, biological day varies according to local climate as illustrated in Sect. 3.2. The phenological development of ragweed before flowering is separated into vegetative and reproductive phases controlled by different factors. Vegetative development stages are germination to seedling emergence (4.5 BD) and emergence to end of juvenile phase (7.0 BD) (Deen et al., 2001). The development rate at the germination to seedling emergence is assumed to be affected

BGD
12, 17595–17641, 2015

by temperature and soil moisture, while the rate at the emergence to end of juvenile phase is affected by temperature alone. From the end of the juvenile phase to the beginning of anthesis (13.5 BD) (Deen et al., 2001) the reproductive development phase takes place and is affected by temperature and photoperiod. Vegetative and reproductive processes are assumed to have an identical response to temperature based on the cardinal temperature determined by Chapman et al. (2014)

$$r_T(T) = \begin{cases} 0 & T < T_{\min} \\ \left(\frac{T - T_{\min}}{T_{\mathrm{opt}} - T_{\min}} \left(\frac{T_{\max} - T}{T_{\max} - T_{\mathrm{opt}}} \right)^{\frac{T_{\max} - T_{\mathrm{opt}}}{T_{\mathrm{opt}} - T_{\min}}} \right)^c & T_{\min} \leq T \leq T_{\max} \\ 0 & T > T_{\max} \end{cases} \tag{7}$$

where $T_{\min}$, T_{opt}, $T_{\max}$ are minimum, optimum, and maximum growing temperatures with values 4.88, 30.65, 42.92 °C respectively. c is a scaling parameter with value of 1.696. All these parameters are derived from growth trail data (Deen et al., 1998a, b, 2001; Shrestha et al., 1999).

The response of development rates to photoperiod is simulated using a modified version of function presented by Chapman et al. (2014)

$$r_L(L) = \begin{cases} e^{(L - 14.0)\ln(1 - L_{\mathrm{s}})} & L \geq 14.0 \\ 1 L < 14.0 \end{cases} \tag{8}$$

where L is day length, expressed in hours. The photoperiod response delays plant development when the day is longer than the threshold photoperiod fixed to 14.0 h (Deen et al., 1998b). L_{s} is a photoperiod sensitivity parameter varying between 0 and 1, which controls development delay and can be adjusted according to sensitivity test to reflect ragweed phenology adapted to local ecological environment. Photoperiods are assumed to affect reproductive development from the end of the juvenile phase.

The response of development rates to soil moisture is assumed to occur from the germination to seedling emergence stage. We use a linear function similar to the one

BGD
12, 17595–17641, 2015

used to account for soil moisture impact on biogenic emission activity factor in MEGAN (Guenther et al., 2012)

$$r_S(\theta) = \begin{cases} 0 & \theta < \theta_w \\ \frac{\theta - \theta_w}{\theta_{opt} - \theta_w} & \theta_w \le \theta \le \theta_1 \\ 1 & \theta > \theta_1 \end{cases} \tag{9}$$

where θ is volumetric water content ($m^3\,m^{-3}$), θ_w ($m^3\,m^{-3}$) is wilting point (the soil moisture level below which plants cannot extract water from soil) and θ_{opt} ($= \theta_w + 0.1$, $m^3\,m^{-3}$) is the optimum soil moisture level in the seed zone over which the development rate reaches maximum (Deen et al., 2001).

According to this phenology model, a total of about 25 BD are theoretically needed to reach the beginning of pollen season BD_{fs} from the initiation date of BD accumulation. However this model relies on parameters determined from controlled conditions and transposition to natural environment is not straightforward in order to calculate a realistic BD_{fs}. Moreover, the model does not allow calculating a priori the end of season date BD_{fe} required in Eq. (5). While we do rely on BD to represent the pheonolgical evolution within the season, we however constrained the starting and ending biological days of the season (BD_{fs} and BD_{fe}) based on observations, as explained hereafter.

2.7.2 Dates of the flowering season

Experimentally, pollen season can be defined in a number of ways from observed pollen concentrations and listed for example in Jato et al. (2006). A widely used definition is the period during which a given percentage of the yearly pollen sum is reached. Another definition refers to the period between the first and last day with pollen concentrations exceeding a specific level. Looking at the temporal distribution of observations, particularly long distribution tails can be found in some cases at the beginning and the end of the pollen season, especially in stations where pollen levels are moderate.

BGD
12, 17595–17641, 2015

This makes the definition of pollen season rather imprecise, while it is in general more constrained in areas with high yearly pollen sum. In our approach, we define the start of the pollen season from 46 observation stations (described in Sect. 2.1) as: the first day of a series of three days in a weekly window for which the pollen concentrations exceed 5 grains m^{-3}, and after 2.5 % of the yearly pollen sum has been reached. The end of the pollen season is defined as: the last day of a series of three days in a weekly window for which the pollen concentrations exceed 5 grains m^{-3}, just before reaching 97.5 % of the yearly pollen sum. (5 grains m^{-3} is supposed the minimum threshold to induce medically relevant risks). The centre of the pollen season is simply defined as the time when the yearly pollen sum reaches 50 %. Kriging method is then used to spatially interpolate pollen season dates determined for each station over the simulation domain. For each grid cell, BD_{fs} and BD_{fm} are determined by simulating and accumulating biological days up to the experimentally defined starting and mid-season dates. Ending season dates is calculated as $2BD_{fm} - BD_{fs}$ according Eq. (5). This methodology requires again a pre-calculation run of RegCM-CLM4.5 where simulated BD is output in order to be matched with observed season dates for each year. Once this step is achieved, spatially resolved BD_{fs} and BD_{fe} can be obtained by averaging across the years and used to perform the integrated pollen run.

2.8 Instantaneous release factor

In Eq. (2), the K_e factor accounts for short term modulation of pollen flux from meteorological conditions. Following Sofiev et al. (2013) K_e is a function of wind speed, relative humidity, and precipitation calculated by RegCM-CLM45 during the run.

$$K_e = \left(\frac{h_{max} - h}{h_{max} - h_{min}}\right) \cdot \left[f_{max} - \exp\left(-\frac{U + w_*}{U_{satur}}\right)\right] \cdot \left(\frac{p_{max} - p}{p_{max} - p_{min}}\right) \tag{10}$$

In this formula, h and p are relative humidity (%) and precipitation (mm h^{-1}), which do not affect the release until lower thresholds (h_{min}, p_{min}) are reached. After reaching upper thresholds (h_{max}, p_{max}) the pollen release is totally inhibited. U is the interactive 10 m wind speed ($m\,s^{-1}$) connected to RegCM prognostic wind and surface roughness, w_* is convective velocity scale ($m\,s^{-1}$), U_{satur} is the saturation wind speed ($m\,s^{-1}$), and f_{max} is the maximum value that wind can contribute to the release rate. The definitions of threshold parameters are discussed in detail in Sofiev et al. (2013).

3 Model application and evaluation

3.1 First guess simulation and calibration of the ragweed density

A first pollen run is performed using the first guess ragweed density described in Sect. 2 and displayed in Fig. 3. First guess density map shows maxima of ragweed in the south-east of France, Benelux countries, and central Europe regions. When comparing the resulting field to observation, simulated concentrations obtained with the first guess distribution are generally overestimated over France, Switzerland and Germany, underestimated in parts of central Europe, and have comparable order of magnitude over some Italian and Croatian stations (Fig. 4). These important biases are in large part due to assumptions made in the construction of the first guess plant density distribution. In order to reduce these biases we perform a model calibration by introducing a correction to the first guess ragweed distribution. For each station, calibration coefficients are obtained by minimizing the yearly root mean square error (RMSE) after constraining the decadal (2000–2010) mean simulated pollen concentration to match the decadal mean observed concentrations (2000–2010) within an admissible value. Calibration coefficients obtained over each station are then interpolated spatially on the domain using ordinary Kriging technique. Then a calibrated simulation using the calibrated density distribution is carried out and repeated several times. After three iterations, the correlation of yearly totals across observation stations increase from 0.23 to 0.98 and the patterns are clustering around the 1 : 1 line (Fig. 4).

The final calibrated ragweed distribution (Fig. 3) shows high density in central Europe including Hungary, Serbia, Bosnia and Herzegovina, Croatia, and western Romania, northern Italy, west France, and also in southern Netherland and northern Belgium. The calibration adjusts the density over all the grid cells with ragweed presence by a factor ranging between 0.1 and 4.4 with an average of 0.98.

The average annual pollen production from 2000 to 2010 (Fig. 5) using the corrected ragweed distribution can reach 1.0^8 grains m^{-2}. The production generally follows the density distribution map with highest flux in central Europe, northern Italy, west France, southern Netherland, and northern Belgium. The annual total pollen concentrations at surface can reach over 20 000 grains m^{-3} with an average 242 grains m^{-3} over the model domain (average for grids with concentrations exceed 1.0 grains m^{-3}). The highest amounts of pollen are present in the central Europe on the Pannonian plain, and noticeable amounts are also shown in northern Italy, west France, southern Netherland, and northern Belgium. We note that the maximum on the Pannonian plain can also be strengthen by a weak synoptic wind ventilation which in principle favours regional accumulation of pollens.

Other than this method, another calibration procedure used in the pollen simulation (Hamaoui-Laguel et al., 2015) by chemistry-transport model CHIMERE is tested. Calibration coefficients calculated from each station are subsequently averaged on each group and then extrapolated over the model grid. The obtained Pearson correlation of 0.74 between observed and modelled yearly totals is in the same order as what from CHIMERE. The calibration is proved to be robust through validation (Hamaoui-Laguel et al., 2015). In this paper, we focus on using the best model configuration given available observations. We do use calibration coefficients obtained from every station instead of grouped ones. Note that through correction, other systematic sources of errors possibly affecting the modelling chain might also be implicitly corrected, leading to undesirable error compensations. However, after running additional tests (not shown here) i.e. by varying model dynamical boundary conditions, a relatively small impact on model performance is found in comparison to the ragweed density distribution impact.

BGD
12, 17595–17641, 2015

3.2 Simulation of pollen season

The simulated start dates, central dates, and end dates of pollen season are averaged from 2000 to 2010 and presented in Fig. 6. The pollen season generally show a positive gradient from the south to the north and from low altitude to high altitude, resulting from the combined effects of temperature, day length, and soil moisture. The start date varies between 21 July and 8 September. Flowering starts in the central European source regions earlier than in west and north of source regions. The central dates occur between 1 August and 27 September, without noticeable difference between central and west source regions. Flowering ends in the central later than in the west of source regions. The pollen season is longest in the central main source regions.

Figure 7 shows the statistical correlation between simulated and observed ragweed pollen start, central, and end dates. The model can reproduce start and central dates better than end dates. Goodness-of-fit tests show that the models account for 68.6, 39.2, and 34.3 % of the observed variance in start, central, and end dates. The RMSE is 4.7, 3.9, and 7.0 days for the pollen start, central, and end dates, respectively. The model reproduces the pollen season in the main source regions fairly well (Fig. 8), where the averaged differences between the simulated and observed pollen season progression are less or equal to 3 days and RMSE is lower than 6 days. For the areas with lower ragweed infestation the results vary widely. The starting dates and central dates are still reproduced well for a majority of the stations while the end dates are more problematic with averaged differences above 6–10 days and RMSE over 8–12 days at some stations. This might result from patchy local ragweed distribution and the contribution of long range transport of pollen, which contributes to the determination of pollen season dates and are representative of local flowering as assumed in our approach. Some stations also stop pollen measurement before the actual end of pollen season which leads to a lower accuracy season ending date.

BGD
12, 17595–17641, 2015

3.3 Model performance and evaluation

The evaluation of the model performance is made by comparing the modelled to observed airborne pollen concentrations over the 2000–2010 period. In the Taylor diagram on Fig. 9, we present an overview on how the models perform in terms of spatio-temporal correlations, standard deviations, and RMSEs compared to observations. The statistics are given for different time scales of variability: daily, annual, or for the full 11 years period (in this case, it is equivalent to spatial statistics only). Different variables are analyzed: the daily concentrations, the annual concentration sums, means, and maxima, and the 11 years concentration sum, mean, and maxima. To plot all the statistics on a single diagram, standard deviation and RMSE are normalized by the standard deviation of observations at the relevant spatiotemporal frequency: observations are thus represented by point OBS on the diagram (perfect correlation coefficient, RMSE = 0 and normalized standard deviation = 1). The closer a point to the reference OBS, the best is the model skill for this particular variable. From the diagram, we can see that:

The model tends to perform very well when the variability is purely spatial and concentrations averages over the 11 year period (dots 5, 6 are very close to OBS). That means the uncertainties about ragweed habitat and its pollen production are reduced to a large extent by the calibration procedure. However, the calibrated simulations do not capture the concentration maximum as well and tend to underestimate the measured spatial standard deviation (decade maximum dot 7 and also for the annual maximum dot 4). The model performs less well but still shows some realism when the variability is involved in both spatial and temporal correlations. The yearly statistics, which reflect the interannual variation of pollen concentrations over the stations, are captured well with correlation coefficients all above 0.80 and normalised standard deviations of 0.89, 0.88, and 0.61 for concentration sum, mean, and maximum respectively. When scores are calculated for daily concentrations over all the stations, the overall spatial–temporal correlation coefficient reaches 0.69 for a relative standard deviation of 0.80.

BGD
12, 17595–17641, 2015

Daily variability is obviously the most difficult to simulate but at the same time might be the most relevant in term of pollen health impact. To investigate further this point, the model performance is regionally evaluated with both discrete and categorical statistical indicators as listed in Zhang et al. (2012). The discrete indicators considered in this study include correlation coefficient, normalized mean bias factors (NMBF), normalized mean error factors (NMEF), mean fractional bias (MFB), and mean fractional error (MFE). NMBF $\leq \pm 0.25$ and NMEF ≤ 0.35 are proposed by Yu et al. (2006) as a criteria of good model performance. Boylan and Russell (2006) recommended MFB $\leq \pm 0.30$ and MFE $\leq \pm 0.50$ as good performance and MFB $\leq \pm 0.60$ and MFE $\leq \pm 0.75$ as acceptable performance for particulate matter pollution. All metrics are computed over daily time series at each station and on whole European domain (Table 1). For the whole domain, the average values of NMBF, NMEF, MFB, and MFE are −0.11, 0.83, −0.15, and −0.31, respectively. Except for NMEF, the indices fall in the range of good performance according to above criteria. The pollen concentrations over the whole domain are slightly underestimated by a factor of 1.11 based on NMBF. As a measure of absolute gross error, NMEF characterize the spread of the deviation between simulations and observations. Although a relatively large gross error of 0.83 exists, the NMEF obtained here is consistent with what is expected from operational air quality models (Yu et al., 2006; Zhang et al., 2006).

The spatial distributions of correlation coefficient, NMBF, NMEF are shown in Fig. 10. The correlations between simulated and observed daily time series are above 0.6–0.7 in the central Europe source region and are mostly above 0.5–0.6 in the source regions of northern Italy and eastern France, while the correlations are low in areas without strong local emission where the majority of observed pollen may originate from long range transport or sporadic ragweed sources. Overall 56.8 % of the stations show a NMBF within ±0.25 and 79.5 % are within ±0.50. In the source regions of central Europe and eastern France, almost all NMBF values lie within ±0.25. In northern Italy the model mostly overestimates the mean daily pollen concentrations by factors ranging from 1.25 to above 2.0 (except for ITMAGE station). Simultaneous overestimation and underestimation can be found for neighbouring stations, which reflects probably the influence of local and patchy sources difficult to account for at 50 km resolution. Better performances are obtained for central European source regions, where the majority of NMEF are within 1.0. Performance degrades in France, where most NMEF values are within 1.2. Simulations are more problematic over northern Italy, where values of NMEF are often above 1.2. Generally 51.4 % of the stations with NMEF are within 1.0 and 79.5 % are within 1.4.

A Categorical evaluation is done by classifying the values of pollen concentration with regard to the thresholds of 5, 20, and 50 grains m^{-3}. Hit rates (fraction of correctly simulated exceedances out of all observed exceedances) and false alarm ratio (fraction of incorrectly simulated exceedances out of all simulated exceedances) are calculated from daily time series over the period. On the whole domain, hit rates for these thresholds are 67.9, 73.3, and 74.3 % and false alarm ratios are 33.3, 31.9, and 32.2 %, respectively. The model tends to perform better for high threshold exceedance while gives more false alarms for lower threshold. As shown on Fig. 11, there are however large regional differences in model performance. Over central European source region, correct prediction often exceed 80 % at moderate and high thresholds and false alarms are about 10 % at low and moderate thresholds and 20 % at high threshold. Performance degrades in France and northern Italy source regions, where correct predictions are mostly around 50–70 % at low and moderate thresholds but false alarms are generally high, especially at moderate threshold.

3.4 Ragweed pollen distribution pattern and risk assessments

With a reasonable confidence in model results, risks region can be identified over the domain. Risk is defined from certain health relevant concentration thresholds: first we can consider minimum ragweed concentrations triggering an allergic reaction. These thresholds are based on experiments involving short exposure time to pollen and then extrapolated in order to define health thresholds in term of daily average concentrations. It is not known, whether a short-time exposure to a large pollen concentra-

BGD
12, 17595–17641, 2015

tion is equivalent to the same dose when less pollen is inhaled over a longer period. Furthermore, these thresholds vary largely between different region and ethnic group. The likely range of such daily thresholds is 5–20 grains m^{-3} day^{-1} estimated by Oswalt and Marshall (2008). Very sensitive people can be affected by as few as 1–2 pollen grains m^{-3} day^{-1} (Bullock et al., 2012).

On this basis, simulated surface concentrations are post-processed to produce 24 h average concentrations. The footprints of ragweed pollen risk are then obtained by selecting the yearly and monthly maximum from daily averaged concentrations. The yearly and monthly maximums are averaged over the decade (2000–2010) to produce footprints depicted in Figs. 12 and 13. The risk is divided into 16 levels to reflect the range of health relevant threshold used in different countries and regions as listed in Table 4.3 of Bullock et al. (2012). The numbers of grid cells at different threshold risk levels are given in Table 2. Hereafter we select some of the representative risk levels to be discussed in more details. From annual footprint of ragweed pollen spread risk, the area with concentration ≥ 1 grains m^{-3} occupies almost 50.3 % area of domain, with an average concentration of 23.7 grains m^{-3}. The risk pattern extends from European mainland to the seas due to the long-range transport. The lowest risk areas with concentration of 1–5 grains m^{-3} are located over the sea as well as in the countries upwind and far from the known sources, such as Spain, UK, Poland, Belarus, and Latvia. The low risk areas with concentration of 5–20 grains m^{-3} are found on the periphery of the source regions and over Mediterranean Sea, occupying 18.2 % of domain. The intermediate risk areas with concentration of 20–50 grains m^{-3} are close to the sources, taking up 6.1 % of domain. The areas with very strong stress ≥ 50 grains m^{-3} are concentrated on main sources, taking up 5.2 % of domain.

Temporally, the pollen risk is determined by seasonal evolution (Fig. 13). August is in general the month contributing the most to the annual risk footprint, with an average concentration of 25.6 grains m^{-3} (from grid cells with concentration above 1 grains m^{-3}). However for some northern region like Belgium and Germany, the maximum risk is found for September (Fig. 13). Overall September shows still important levels 18.9 grains m^{-3} when October and July exhibits much weaker concentrations. The risk areas associated to pollen for each month are given in Table 2.

Besides the triggering of allergic reactions at a certain threshold, the time of exposure above a certain threshold might be also important e.g. in term of sensitisation to ragweed pollen. To assess a risk based on this criterion, exposure time, expressed as the decadal average of the number of days per season above a certain threshold, are calculated and reported in Fig. 14. Relevant threshold are 5, 10, 20, 50 grain m^{-3}.

The longest exposure times occurs in Pannonian Plain at all thresholds, reaching for example about 30 days above 20 grains m^{-3}. Northern Italy and France can also show some important exposure time. Over the measurement stations, we can compare measured and simulated exposure time at different thresholds as reported in Fig. 14, where measurements are indicated with circles coloured by the measured number of days (left half) and corresponding simulated number of days (right half). Simulated and measured risk agrees reasonably for most stations with in general better comparison for moderate thresholds (10 and 20 grain m^{-3}) relative to high or low thresholds. Nevertheless except for a few stations the simulated exposure time tends to be overestimated.

4 Summary and conclusions

This study presents a regional-climatic simulation framework based on RegCM4 for investigating the dynamics of emissions and transport of ragweed pollen. The RegCM-pollen modelling system incorporates a pollen emission module coupled to CLM4.5 and a transport module as part of the chemistry transport component of RegCM. The emission module is designed to calculate online pollen release based on plant density distribution, species-specific phenology, pollen production, flowering probability and modulation by short-term meteorological conditions. Once released, pollens are considered as monodisperse aerosol undergoing classical transport and deposition processes. This approach allows dynamical response of pollen ripening, release, and dispersion to key environmental driver like temperature, photoperiod, soil moisture, precipitation, relative humidity, turbulence, and wind. Through the pollen production link to NPP, other environmental and climate relevant factors as atmospheric CO_2 concentrations are also accounted for. The specific ragweed phenology is parameterized from growth controlled experiment but has to be somehow adjusted to observations for more realism of the flowering season simulations over Europe. Similarly, ragweed spatial distribution is a very poorly constrained parameter which has to be corrected through a calibration procedure. The calibration increases the spatial correlation over the decade from 0.23 to 0.98 and the spatial temporal correlation of simulated and measured daily concentrations from 0.28 to 0.69.

The RegCM-pollen framework is applied to the European domain for the period 2000–2010. Comparing with the observed flowering season, the model can reproduce start dates and central dates well, with 68.6, 39.2 % of the explained variance and 4.7, 3.9 days of RMSE in start date and central date, respectively. The pollen season in the main source regions are reproduced fairly well while in the areas with lower ragweed infestation the deviations are evident. The model in generally captures the gross features of the pollen concentrations found in Europe. Statistical measures of NMBF, MFB, and MFE over the domain fall in the range of recommendation for a good performance while NMEF is a bit large with a value of 0.83. The model performs better over the central European source region, where the daily correlations at most stations are above 0.6–0.7 and NMEF lie within 1.0. Performance tends to degrade in France and northern Italy. Still, the values of NMEF for pollen simulation are generally consistent with what is expected from operational air quality models for aerosols for example. Categorical evaluation reveals the model tends to give better predictions for high threshold while gives more false alarms for low threshold. A better performance is also shown over the central European source region at all levels, with correct prediction are above 80 % and false alarms are within 20 %.

The multi-annual average footprints of ragweed pollen spread risk are produced from calibration simulations. The pollen plume with concentration ≥ 1 grains m^{-3} can reach on the seas far away from European mainland. The risk areas with concentration above

BGD
12, 17595–17641, 2015

5 grains m^{-3} are around the source and on Mediterranean Sea, occupying total 29.5 % of domain. While the areas with very strong stress ≥ 50 grains m^{-3} are confined in narrow source areas. From the seasonal distribution, August in general contributes most to the annual footprint and September shows still important levels. The longest risk exposure time occurs on Pannonian Plain at all thresholds. Northern Italy and France also show some considerable exposure time.

The modelling framework presented here allows simultaneous estimation of ragweed pollen risk both for hindcast simulations (including sensitivity studies to different parameters) and for study of potential risk evolution changes under future-climate scenarios as illustrated in Hamaoui-Laguel et al. (2015). Still a long list of uncertainties hinders an accurate estimate of the airborne pollen patterns and risk within presented framework. A better understanding of phenological process, production potential, plant distribution and the dynamic response of release rate to meteorological conditions will help to reduce these uncertainties and improve the model performance.

Acknowledgements. This research is funded by the European Union's Seventh Framework Programme (FP7/2007-2013) under grant agreements no 282687 Atopica (http://cordis.europa.eu/fp7). We thank the contributors of ragweed distribution data. Pollen observation data are kindly provided by the European Aeroallergen Network, Reseau National de Surveillance Aerobiologique, ARPA-Veneto, ARPA-FVG, and Croatian monitoring sites.

References

Allard, H. A.: Flowering behaviour and natural distribution of the eastern ragweeds (Ambrosia) as affected by length of day, Ecology, 26, 387–394, 1945.

Boylan, J. W. and Russell, A. G.: PM and light extinction model performance metrics, goals, and criteria for three-dimensional air quality models, Atmos. Environ., 40, 4946–4959, doi:10.1016/j.atmosenv.2005.09.087, 2006.

Bullock, J. M., Chapman, D., Schafer, S., Roy, D., Girardello, M., Haynes, T., Beal, S., Wheeler, B., Dickie, I., Phang, Z., Tinch, R., Čivić, K., Delbaere, B., Jones-Walters, L., Hilbert, A., Schrauwen, A., Prank, M., Sofiev, M., Niemelä, S., Räisänen, P., Lees, B., Skin-

BGD

12, 17595–17641, 2015

Estimates of common ragweed pollen emission and dispersion

L. Liu et al.

ner, M., Finch, S., and Brough, C.: Assessing and controlling the spread and the effects of common ragweed in Europe, Final Report ENV.B2/ETU/2010/0037, European Commission, 456 pp., 2012.

Burbach, G. J., Heinzerling, L. M., Röhnelt, C., Bergmann, K.-C., Behrendt, H., and Zuberbier, T.: Ragweed sensitization in Europe – GA(2)LEN study suggests increasing prevalence, Allergy, 64, 664–665, doi:10.1111/j.1398-9995.2009.01975.x, 2009.

Cecchi, L., Morabito, M., Domeneghetti, M. P., Crisci, A., Onorari, M., and Orlandini, S.: Long distance transport of ragweed pollen as a potential cause of allergy in central Italy, Ann. Allerg. Asthma Im., 96, 86–91, doi:10.1016/S1081-1206(10)61045-9, 2006.

Chapman, D. S., Haynes, T., Beal, S., Essl, F., and Bullock, J. M.: Phenology predicts the native and invasive range limits of common ragweed, Global Change Biol., 20, 192–202, doi:10.1111/Gcb.12380, 2014.

Chauvel, B., Dessaint, F., Cardinal-Legrand, C., and Bretagnolle, F.: The historical spread of *Ambrosia artemisiifolia* L. in France from herbarium records, J. Biogeogr., 33, 665–673, doi:10.1111/j.1365-2699.2005.01401.x, 2006.

D'Amato, G., Cecchi, L., Bonini, S., Nunes, C., Annesi-Maesano, I., Behrendt, H., Liccardi, G., Popov, T., and Van Cauwenberge, P.: Allergenic pollen and pollen allergy in Europe, Allergy, 62, 976–990, doi:10.1111/j.1398-9995.2007.01393.x, 2007.

Dahl, A., Strandhede, S.-O., and Wihl, J.-A.: Ragweed – an allergy risk in Sweden?, Aerobiologia, 15, 293–297, doi:10.1023/A:1007678107552, 1999.

Deen, W., Hunt, L. A., and Swanton, C. J.: Photothermal time describes common ragweed (*Ambrosia artemisiifolia* L.) phenological development and growth, Weed Sci., 46, 561–568, 1998a.

Deen, W., Hunt, T., and Swanton, C. J.: Influence of temperature, photoperiod, and irradiance on the phenological development of common ragweed (*Ambrosia artemisiifolia*), Weed Sci., 46, 555–560, 1998b.

Deen, W., Swanton, C. J., and Hunt, L. A.: A mechanistic growth and development model of common ragweed, Weed Sci., 49, 723–731, doi:10.1614/0043-1745(2001)049[0723:AMGADM]2.0.CO;2, 2001.

Efstathiou, C., Isukapalli, S., and Georgopoulos, P.: A mechanistic modeling system for estimating large-scale emissions and transport of pollen and co-allergens, Atmos. Environ., 45, 2260–2276, doi:10.1016/j.atmosenv.2010.12.008, 2011.

Emanuel, K. A. and Zivkovic-Rothman, M.: Development and evaluation of a convection scheme for use in climate models, J. Atmos. Sci., 56, 1766–1782, 1999.
Fumanal, B., Chauvel, B., and Bretagnolle, F.: Estimation of pollen and seed production of common ragweed in France, Ann. Agr. Env. Med., 14, 233–236, 2007.
Gallinza, N., Barić, K., Šćepanović, M., Goršić, M., and Ostojić, Z.: Distribution of invasive weed *Ambrosia artemisiifolia* L. in Croatia, Agriculturae Conspectus Scientificus, 75, 75–81, 2010.
García-Mozo, H., Galán, C., Belmonte, J., Bermejo, D., Candau, P., Díaz de la Guardia, C., Elvira, B., Gutiérrez, M., Jato, V., Silva, I., Trigo, M. M., Valencia, R., and Chuine, I.: Predicting the start and peak dates of the Poaceae pollen season in Spain using process-based models, Agr. Forest Meteorol., 149, 256–262, doi:10.1016/j.agrformet.2008.08.013, 2009.
Giorgi, F., Pal, J. S., Bi, X., Sloan, L., Elguindi, N., and Solmon, F.: Introduction to the TAC special issue: the RegCNET network, Theor. Appl. Climatol., 86, 1–4, doi:10.1007/s00704-005-0199-z, 2006.
Giorgi, F., Coppola, E., Solmon, F., Mariotti, L., Sylla, M. B., Bi, X., Elguindi, N., Diro, G. T., Nair, V., Giuliani, G., Turuncoglu, U. U., Cozzini, S., Güttler, I., O'Brien, T. A., Tawfik, A. B., Shalaby, A., Zakey, A. S., Steiner, A. L., Stordal, F., Sloan, L. C., and Brankovic, C.: RegCM4: model description and preliminary tests over multiple CORDEX domains, Clim. Res., 52, 7–29, doi:10.3354/cr01018, 2012.
Grell, G. A.: Prognostic evaluation of assumptions used by cumulus parameterizations, Mon. Weather Rev., 121, 764–787, doi:10.1175/1520-0493(1993)121<0764:PEOAUB>2.0.CO;2, 1993.
Guenther, A. B., Jiang, X., Heald, C. L., Sakulyanontvittaya, T., Duhl, T., Emmons, L. K., and Wang, X.: The Model of Emissions of Gases and Aerosols from Nature version 2.1 (MEGAN2.1): an extended and updated framework for modeling biogenic emissions, Geosci. Model Dev., 5, 1471–1492, doi:10.5194/gmd-5-1471-2012, 2012.
Hamaoui-Laguel, L., Vautard, R., Liu, L., Solmon, F., Viovy, N., Khvorostyanov, D., Essl, F., Chuine, I., Colette, A., Semenov, M. A., Schaffhauser, A., Storkey, J., Thibaudon, M., and Epstein, M. M.: Effects of climate change and seed dispersal on airborne ragweed pollen loads in Europe, Nature Clim. Change, 5, 766–771, doi:10.1038/nclimate2652, 2015.
Helbig, N., Vogel, B., Vogel, H., and Fiedler, F.: Numerical modelling of pollen dispersion on the regional scale, Aerobiologia, 20, 3–19, doi:10.1023/B:AERO.0000022984.51588.30, 2004.
Hirst, J. M.: An automatic volumetric spore trap, Ann. Appl. Biol., 39, 257–265, 1952.

BGD
12, 17595–17641, 2015

Title Page
Abstract Introduction
Conclusions References
Tables Figures
◂ ▸
Back Close
Full Screen / Esc
Printer-friendly Version
Interactive Discussion

Holtslag, A. A. M., De Bruijn, E. I. F., and Pan, H.-L.: A high-resolution air-mass transformation model for short-range weather forecasting, Mon. Weather Rev., 118, 1561–1575, doi:10.1175/1520-0493(1990)118<1561:AHRAMT>2.0.CO;2, 1990.

Hurtt, G. C., Frolking, S., Fearon, M. G., Moore, B., Shevliakova, E., Malyshev, S., Pacala, S. W., and Houghton, R. A.: The underpinnings of land-use history: three centuries of global gridded land-use transitions, wood-harvest activity, and resulting secondary lands, Global Change Biol., 12, 1208–1229, doi:10.1111/j.1365-2486.2006.01150.x, 2006.

Jato, V., Rodriguez-Rajo, F. J., Alcázar, P., De Nuntiis, P., Galán, C., and Mandrioli, P.: May the definition of pollen season influence aerobiological results?, Aerobiologia, 22, 13–25, doi:10.1007/s10453-005-9011-x, 2006.

Kazinczi, G., Béres, I., Pathy, Z., and Novák, R.: Common ragweed (*Ambrosia artemisiifolia* L.): a review with special regards to the results in Hungary: II. Importance and harmful effect, allergy, habitat, allelopathy and beneficial characteristics, Herbologia, 9, 93–117, 2008.

Martin, M. D., Chamecki, M., and Brush, G. S.: Anthesis synchronization and floral morphology determine diurnal patterns of ragweed pollen dispersal, Agr. Forest Meteorol., 150, 1307–1317, doi:10.1016/j.agrformet.2010.06.001, 2010.

Meleux, F., Solmon, F., and Giorgi, F.: Increase in summer European ozone amounts due to climate change, Atmos. Environ., 41, 7577–7587, doi:10.1016/j.atmosenv.2007.05.048, 2007.

Oleson, K. W., Lawrence, D. M., Bonan, G. B., Drewniak, B., Huang, M., Koven, C. D., Levis, S., Li, F., Riley, W. J., Subin, Z. M., Swenson, S. C., Thornton, P. E., Bozbiyik, A., Fisher, R., Heald, C. L., Kluzek, E., Lamarque, J.-F., Lawrence, P. J., Leung, L. R., Lipscomb, W., Muszala, S., Ricciuto, D. M., Sacks, W., Sun, Y., Tang, J., and Yang, Z.-L.: Technical description of version 4.5 of the Community Land Model (CLM), NCAR Technical Note NCAR/TN-503+STR, National Center for Atmospheric Research, Boulder, Colorado, 434 pp., 2013.

Oswalt, M. L. and Marshall, G. D.: Ragweed as an example of worldwide allergen expansion, Allergy Asthma Clin. Immunol., 4, 130–135, doi:10.1186/1710-1492-4-3-130, 2008.

Pal, J. S., Small, E. E., and Eltahir, E. A. B.: Simulation of regional-scale water and energy budgets: representation of subgrid cloud and precipitation processes within RegCM, J. Geophys. Res.-Atmos., 105, 29579–29594, doi:10.1029/2000JD900415, 2000.

Pal, J. S., Giorgi, F., Bi, X., Elguindi, N., Solmon, F., Rauscher, S. A., Gao, X., Francisco, R., Zakey, A., Winter, J., Ashfaq, M., Syed, F. S., Sloan, L. C., Bell, J. L., Diffenbaugh, N. S., Karmacharya, J., Konaré, A., Martinez, D., da Rocha, R. P., and Steiner, A. L.: Regional climate modeling for the developing world: the ICTP RegCM3 and RegCNET, B. Am. Meteorol. Soc., 88, 1395–1409, doi:10.1175/BAMS-88-9-1395, 2007.

Payne, W. W.: The morphology of the inflorescence of ragweeds (Ambrosia-Franseria: compositae), Am. J. Bot., 50, 872–880, doi:10.2307/2439774, 1963.

Pinke, G., Karácsony, P., Czúcz, B., and Botta-Dukat, Z.: Environmental and land-use variables determining the abundance of *Ambrosia artemisiifolia* in arable fields in Hungary, Preslia, 83, 219–235, 2011.

Prank, M., Chapman, D. S., Bullock, J. M., Belmonte, J., Berger, U., Dahl, A., Jager, S., Kovtunenko, I., Magyar, D., Niemela, S., Rantio-Lehtimaki, A., Rodinkova, V., Sauliene, I., Severova, E., Sikoparija, B., and Sofiev, M.: An operational model for forecasting ragweed pollen release and dispersion in Europe, Agr. Forest Meteorol., 182, 43–53, doi:10.1016/j.agrformet.2013.08.003, 2013.

Rogers, C. A., Wayne, P. M., Macklin, E. A., Muilenberg, M. L., Wagner, C. J., Epstein, P. R., and Bazzaz, F. A.: Interaction of the onset of spring and elevated atmospheric CO_2 on ragweed (*Ambrosia artemisiifolia* L.) pollen production, Environ. Health Persp., 114, 865–869, doi:10.1289/ehp.8549, 2006.

Shalaby, A., Zakey, A. S., Tawfik, A. B., Solmon, F., Giorgi, F., Stordal, F., Sillman, S., Zaveri, R. A., and Steiner, A. L.: Implementation and evaluation of online gas-phase chemistry within a regional climate model (RegCM-CHEM4), Geosci. Model Dev., 5, 741–760, doi:10.5194/gmd-5-741-2012, 2012.

Shrestha, A., Roman, E. S., Thomas, A. G., and Swanton, C. J.: Modeling germination and shoot-radicle elongation of *Ambrosia artemisiifolia*, Weed Sci., 47, 557–562, 1999.

Šikoparija, B., Skjøth, C. A., Radišić, P., Stjepanivić, B., Hrga, I., Apatini, D., Martinez, D., Páldy, A., Ianovici, N., and Smith, M.: Aerobiology data used for producing inventories of invasive species, in: Proceedings of the international symposium on current trends in plant protection, Belgrade, Serbi, 8 September 2012, 7–14, 2012.

Šikoparija, B., Skjøth, C. A., Kübler, K. A., Dahl, A., Sommer, J., Grewling, Ł., Radišić, P., and Smith, M.: A mechanism for long distance transport of Ambrosia pollen from the Pannonian Plain, Agr. Forest Meteorol., 180, 112–117, doi:10.1016/j.agrformet.2013.05.014, 2013.

Simard, M. J. and Benoit, D. L.: Effect of repetitive mowing on common ragweed (*Ambrosia Artemisiifolia* L.) pollen and seed production, Ann. Agr. Env. Med., 18, 55–62, 2011.

Simard, M. J. and Benoit, D. L.: Potential pollen and seed production from early- and late-emerging common ragweed in corn and soybean, Weed Technol., 26, 510–516, 2012.

BGD
12, 17595–17641, 2015

Estimates of common ragweed pollen emission and dispersion

L. Liu et al.

Skjøth, C. A.: Integrating measurements, phenological models and atmospheric models in aerobiology, PhD thesis, Copenhagen University and National Environmental Research Institute, Denmark, 123 pp., 2009.
Skjøth, C. A., Smith, M., Šikoparija, B., Stach, A., Myszkowska, D., Kasprzykf, I., Radišić, P., Stjepanović, B., Hrga, I., Apatini, D., Magyar, D., Páldy, A., and Ianovici, N.: A method for producing airborne pollen source inventories: an example of Ambrosia (ragweed) on the Pannonian Plain, Agr. Forest Meteorol., 150, 1203–1210, doi:10.1016/j.agrformet.2010.05.002, 2010.
Smith, M., Skjøth, C. A., Myszkowska, D., Uruska, A., Puc, M., Stach, A., Balwierz, Z., Chlopek, K., Piotrowska, K., Kasprzyk, I., and Brandt, J.: Long-range transport of Ambrosia pollen to Poland, Agr. Forest Meteorol., 148, 1402–1411, doi:10.1016/j.agrformet.2008.04.005, 2008.
Smith, M., Cecchi, L., Skjøth, C. A., Karrer, G., and Šikoparija, B.: Common ragweed: a threat to environmental health in Europe, Environ. Int., 61, 115–126, doi:10.1016/j.envint.2013.08.005, 2013.
Sofiev, M., Siljamo, P., Ranta, H., and Rantio-Lehtimäki, A.: Towards numerical forecasting of long-range air transport of birch pollen: theoretical considerations and a feasibility study, Int. J. Biometeorol., 50, 392–402, doi:10.1007/s00484-006-0027-x, 2006.
Sofiev, M., Siljamo, P., Ranta, H., Linkosalo, T., Jaeger, S., Rasmussen, A., Rantio-Lehtimaki, A., Severova, E., and Kukkonen, J.: A numerical model of birch pollen emission and dispersion in the atmosphere. Description of the emission module, Int. J. Biometeorol., 57, 45–58, doi:10.1007/s00484-012-0532-z, 2013.
Solmon, F., Giorgi, F., and Liousse, C.: Aerosol modelling for regional climate studies: application to anthropogenic particles and evaluation over a European/African domain, Tellus B, 58, 51–72, doi:10.1111/j.1600-0889.2005.00155.x, 2006.
Solmon, F., Elguindi, N., and Mallet, M.: Radiative and climatic effects of dust over West Africa, as simulated by a regional climate model, Clim. Res., 52, 97–113, doi:10.3354/cr01039, 2012.
Stach, A., Smith, M., Skjøth, C. A., and Brandt, J.: Examining Ambrosia pollen episodes at Poznan (Poland) using back-trajectory analysis, Int. J. Biometeorol., 51, 275–286, doi:10.1007/s00484-006-0068-1, 2007.

Storkey, J., Stratonovitch, P., Chapman, D. S., Vidotto, F., and Semenov, M. A.: A process-based approach to predicting the effect of climate change on the distribution of an invasive allergenic plant in Europe, Plos One, 9, e88156, doi:10.1371/journal.pone.0088156, 2014.
Taramarcaz, P., Lambelet, C., Clot, B., Keimer, C., and Hauser, C.: Ragweed (Ambrosia) progression and its health risks: will Switzerland resist this invasion?, Swiss Med. Wkly., 135, 538–548, 2005.
Thornton, P. E., Law, B. E., Gholz, H. L., Clark, K. L., Falge, E., Ellsworth, D. S., Golstein, A. H., Monson, R. K., Hollinger, D., Falk, M., Chen, J., and Sparks, J. P.: Modeling and measuring the effects of disturbance history and climate on carbon and water budgets in evergreen needleleaf forests, Agr. Forest Meteorol., 113, 185–222, doi:10.1016/S0168-1923(02)00108-9, 2002.
Thornton, P. E., Lamarque, J. F., Rosenbloom, N. A., and Mahowald, N. M.: Influence of carbon-nitrogen cycle coupling on land model response to CO_2 fertilization and climate variability, Global Biogeochem. Cy., 21, GB4018, doi:10.1029/2006gb002868, 2007.
Tummon, F., Solmon, F., Liousse, C., and Tadross, M.: Simulation of the direct and semidirect aerosol effects on the southern Africa regional climate during the biomass burning season, J. Geophys. Res.-Atmos., 115, D19206, doi:10.1029/2009JD013738, 2010.
Willemsen, R. W.: Effect of stratification temperature and germination temperature on germination and induction of secondary dormancy in common ragweed seeds, Am. J. Bot., 62, 1–5, doi:10.2307/2442073, 1975.
Yu, S. C., Eder, B., Dennis, R., Chu, S.-H., and Schwartz, S. E.: New unbiased symmetric metrics for evaluation of air quality models, Atmos. Sci. Lett., 7, 26–34, doi:10.1002/asl.125, 2006.
Zakey, A. S., Solmon, F., and Giorgi, F.: Implementation and testing of a desert dust module in a regional climate model, Atmos. Chem. Phys., 6, 4687–4704, doi:10.5194/acp-6-4687-2006, 2006.
Zhang, R., Duhl, T., Salam, M. T., House, J. M., Flagan, R. C., Avol, E. L., Gilliland, F. D., Guenther, A., Chung, S. H., Lamb, B. K., and VanReken, T. M.: Development of a regional-scale pollen emission and transport modeling framework for investigating the impact of climate change on allergic airway disease, Biogeosciences, 11, 1461–1478, doi:10.5194/bg-11-1461-2014, 2014.
Zhang, Y., Liu, P., Queen, A., Misenis, C., Pun, B., Seigneur, C., and Wu, S.-Y.: A comprehensive performance evaluation of MM5-CMAQ for the Summer 1999 Southern Oxidants

Study episode – Part II: Gas and aerosol predictions, Atmos. Environ., 40, 4839–4855, doi:10.1016/j.atmosenv.2005.12.048, 2006.
Zhang, Y., Bocquet, M., Mallet, V., Seigneur, C., and Baklanov, A.: Real-time air quality forecasting, part I: History, techniques, and current status, Atmos. Environ., 60, 632–655, doi:10.1016/j.atmosenv.2012.06.031, 2012.
Zink, K., Vogel, H., Vogel, B., Magyar, D., and Kottmeier, C.: Modeling the dispersion of *Ambrosia artemisiifolia* L. pollen with the model system COSMO-ART, Int. J. Biometeorol., 56, 669–680, doi:10.1007/s00484-011-0468-8, 2012.
Zink, K., Pauling, A., Rotach, M. W., Vogel, H., Kaufmann, P., and Clot, B.: EMPOL 1.0: a new parameterization of pollen emission in numerical weather prediction models, Geosci. Model Dev., 6, 1961–1975, doi:10.5194/gmd-6-1961-2013, 2013.

Table 1. Model performance on simulation of daily average concentrations for 2000–2010.

discrete statistical indicators			
normalized mean bias factors (NMBF)	−0.11		
normalized mean error factors (NMEF)	0.83		
mean fractional bias (MFB)	−0.15		
mean fractional error (MFE)	−0.31		
correlation coefficient (R)	0.69		
categorical statistical indicators (%)	Threshold (grains m^{-3})		
	5	20	50
Hit rates	67.9	73.3	74.3
false alarm ratio	33.3	31.9	32.2

BGD
12, 17595–17641, 2015

Table 2. Percent area with the surface concentration of ragweed pollen at different risk levels, average for 2000–2010.

level	Lower bound of the thresholds/ (grain m^{-3})	Percent area in domain				
		Jul	Aug	Sep	Oct	annual
1	0	99.6	61.1	54.3	92.4	49.7
2	1	0.2	6.8	11.5	2.3	9.1
3	2	0.1	8.8	10.2	2.7	11.7
4	5	0.0	2.5	1.9	0.3	2.1
5	6	0.1	3.1	3.6	0.5	3.8
6	8	0.0	2.1	2.7	0.3	2.9
7	10	0.0	1.0	1.2	0.1	1.3
8	11	0.0	6.8	6.5	0.8	8.1
9	20	0.0	2.6	2.1	0.4	3.5
10	30	0.0	1.3	1.9	0.2	2.6
11	50	0.0	1.2	1.3	0.0	1.6
12	80	0.0	0.4	0.4	0.0	0.6
13	100	0.0	1.1	1.4	0.0	1.4
14	200	0.0	1.0	0.8	0.0	1.2
15	500	0.0	0.2	0.2	0.0	0.3
16	1000	0.0	0.0	0.0	0.0	0.1

BGD
12, 17595–17641, 2015

BGD
12, 17595–17641, 2015

Estimates of common ragweed pollen emission and dispersion

L. Liu et al.

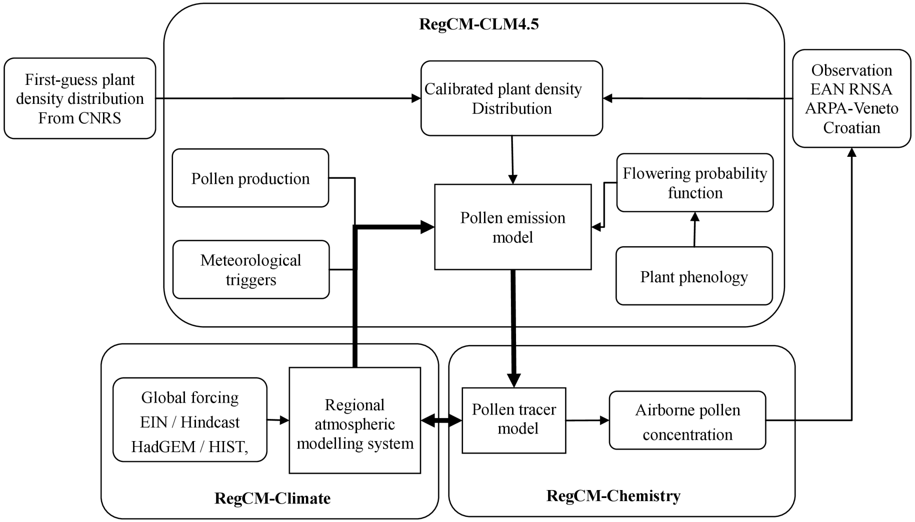

Figure 1. Ragweed pollen modelling within online RegCM-pollen simulation framework.

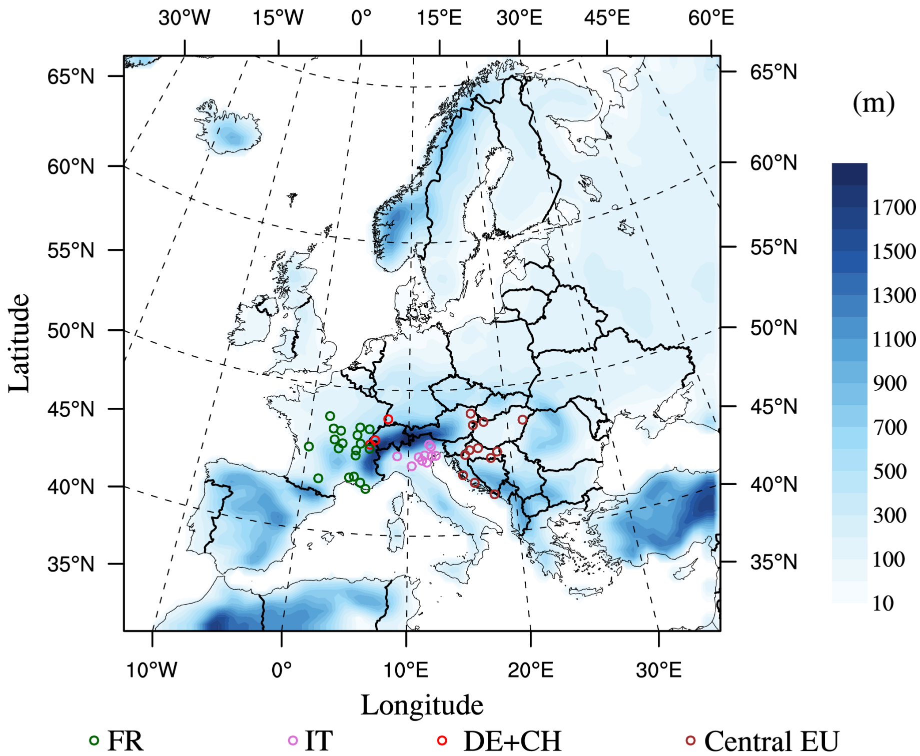

Figure 2. Model domain and the observation sites with topography.

BGD
12, 17595–17641, 2015

Estimates of common ragweed pollen emission and dispersion

L. Liu et al.

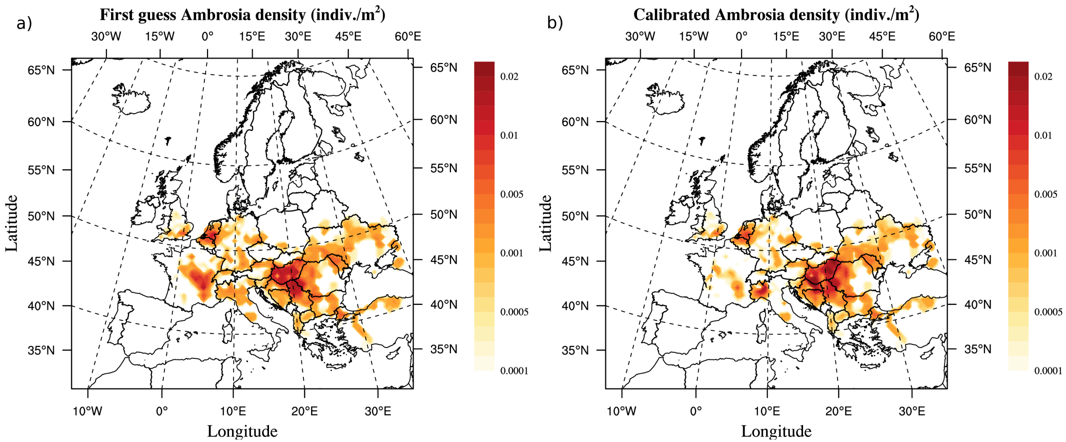

Figure 3. First guess **(a)** and calibrated **(b)** ragweed density distribution.

BGD
12, 17595–17641, 2015

Estimates of common ragweed pollen emission and dispersion

L. Liu et al.

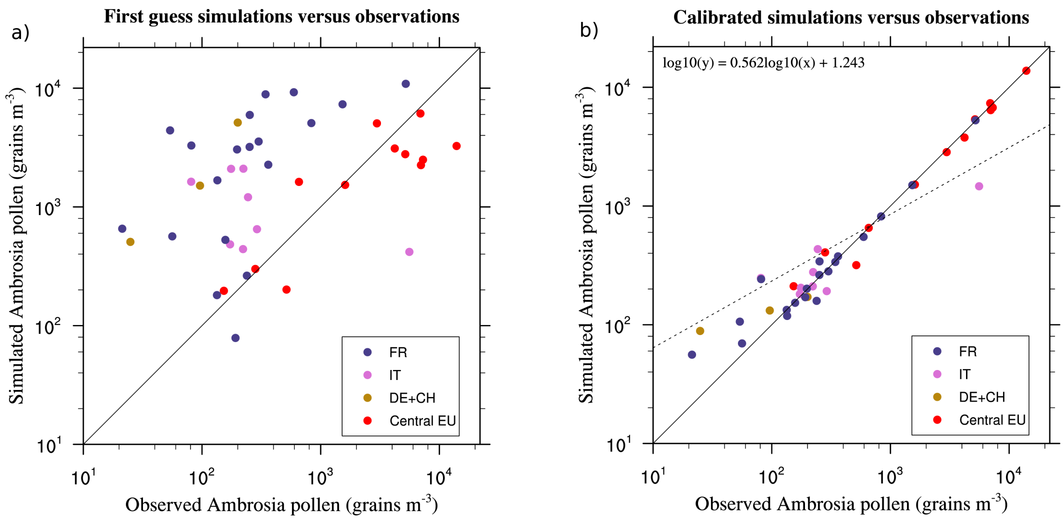

Figure 4. Average (2000–2010) annual pollen sum for first guess **(a)** and calibrated **(b)** simulations on sites.

BGD
12, 17595–17641, 2015

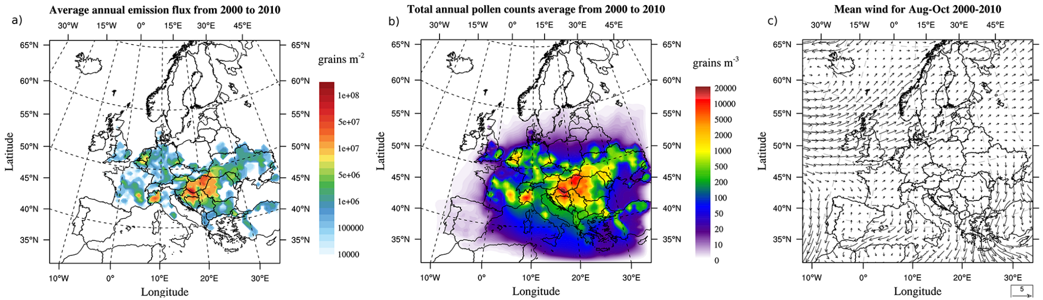

Figure 5. Annual pollen emission fluxes **(a)**, total annual pollen sum (sum of daily mean concentrations) **(b)**, and mean wind for August–October **(c)** average from 2000 to 2010.

Discussion Paper | Discussion Paper | Discussion Paper | Discussion Paper |

BGD

12, 17595–17641, 2015

Estimates of common ragweed pollen emission and dispersion

L. Liu et al.

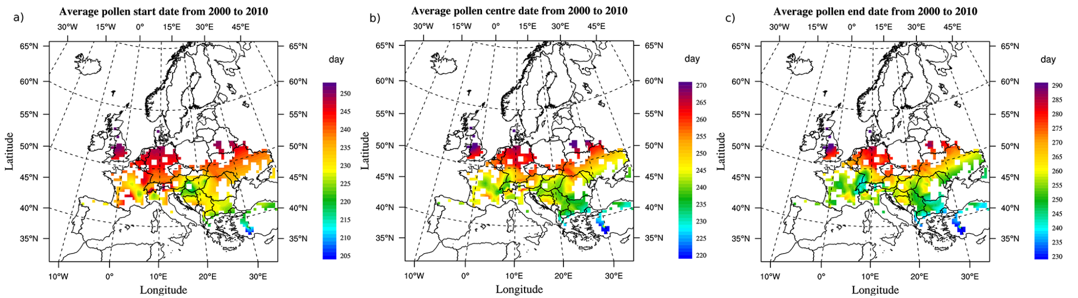

Figure 6. Average pollen season (day of the year) from 2000 to 2010: start dates **(a)**, central date **(b)**, and end dates **(c)**.

BGD
12, 17595–17641, 2015

Estimates of common ragweed pollen emission and dispersion

L. Liu et al.

Title Page
Abstract Introduction
Conclusions References
Tables Figures
◀| |▶
◀ ▶
Back Close
Full Screen / Esc
Printer-friendly Version
Interactive Discussion

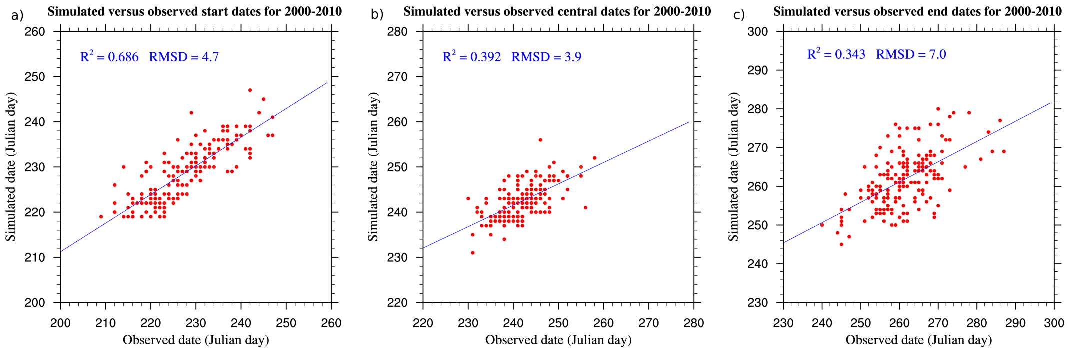

Figure 7. Statistical correlation between simulated and observed ragweed pollen season (day of the year) for 2000–2010: start dates (left), central dates (middle), and end dates (right).

BGD
12, 17595–17641, 2015

Estimates of common ragweed pollen emission and dispersion

L. Liu et al.

Title Page
Abstract Introduction
Conclusions References
Tables Figures
◀I ▶I
◀ ▶
Back Close
Full Screen / Esc
Printer-friendly Version
Interactive Discussion

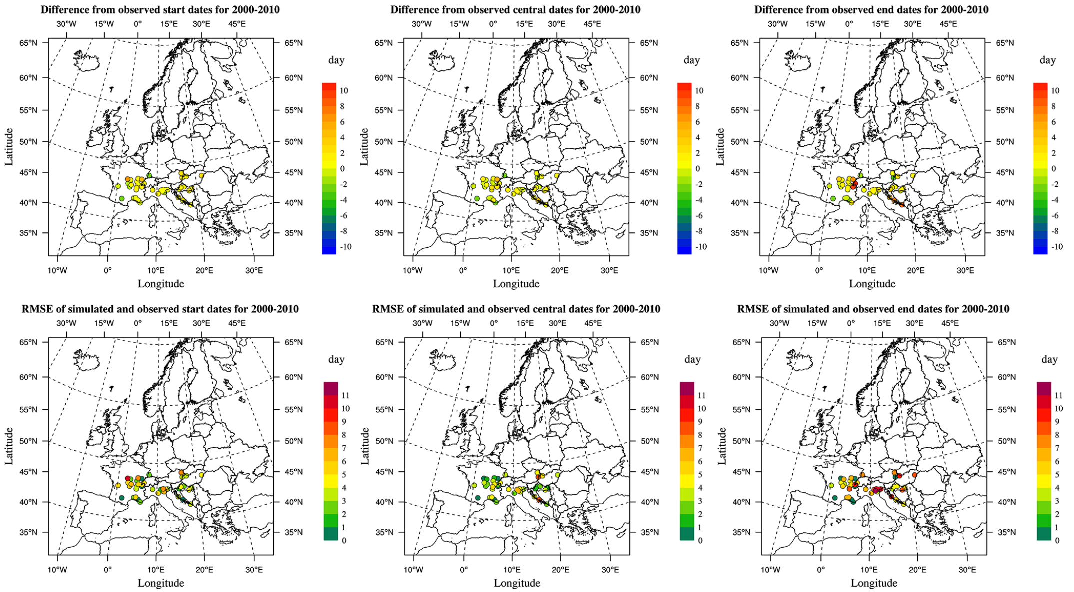

Figure 8. Pollen season accuracy: differences (upper row) and RMSEs (lower row) between the simulated and observed start, central, and end date for 2000–2010.

BGD
12, 17595–17641, 2015

Title Page
Abstract Introduction
Conclusions References
Tables Figures
◀◀ ▶▶
◀ ▶
Back Close
Full Screen / Esc
Printer-friendly Version
Interactive Discussion

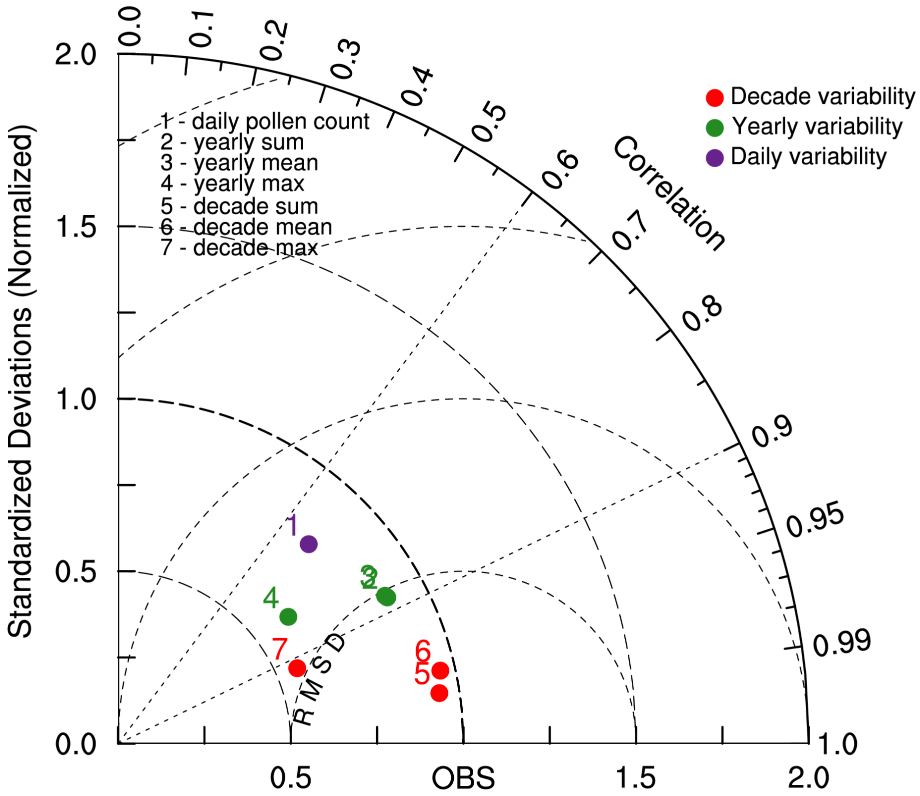

Figure 9. Normalized Taylor diagram showing spatial and temporal correlations coefficients, standard deviations and RMSEs between simulations and observations for the period 2000–2010. Standard deviation and RMSE are normalized by the standard deviation of observations at the relevant spatiotemporal frequency.

BGD
12, 17595–17641, 2015

Estimates of common ragweed pollen emission and dispersion

L. Liu et al.

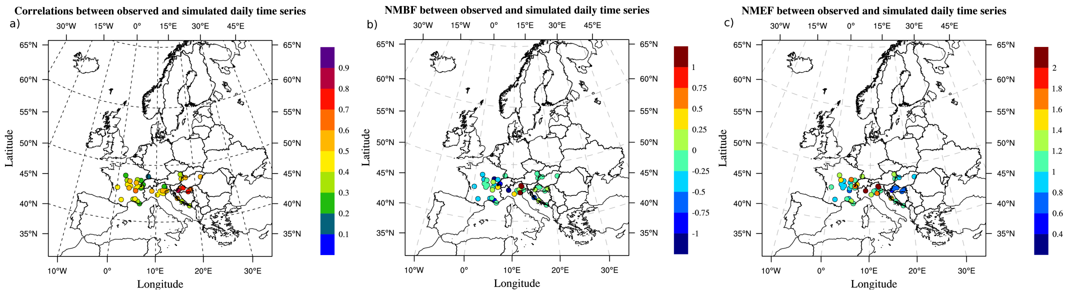

Figure 10. Statistical measures between simulated and observed daily pollen time series for each site: correlation coefficients **(a)**, normalized mean bias factors **(b)** and normalized mean error factors **(c)**.

BGD
12, 17595–17641, 2015

Estimates of common ragweed pollen emission and dispersion

L. Liu et al.

BGD

12, 17595–17641, 2015

Estimates of common ragweed pollen emission and dispersion

L. Liu et al.

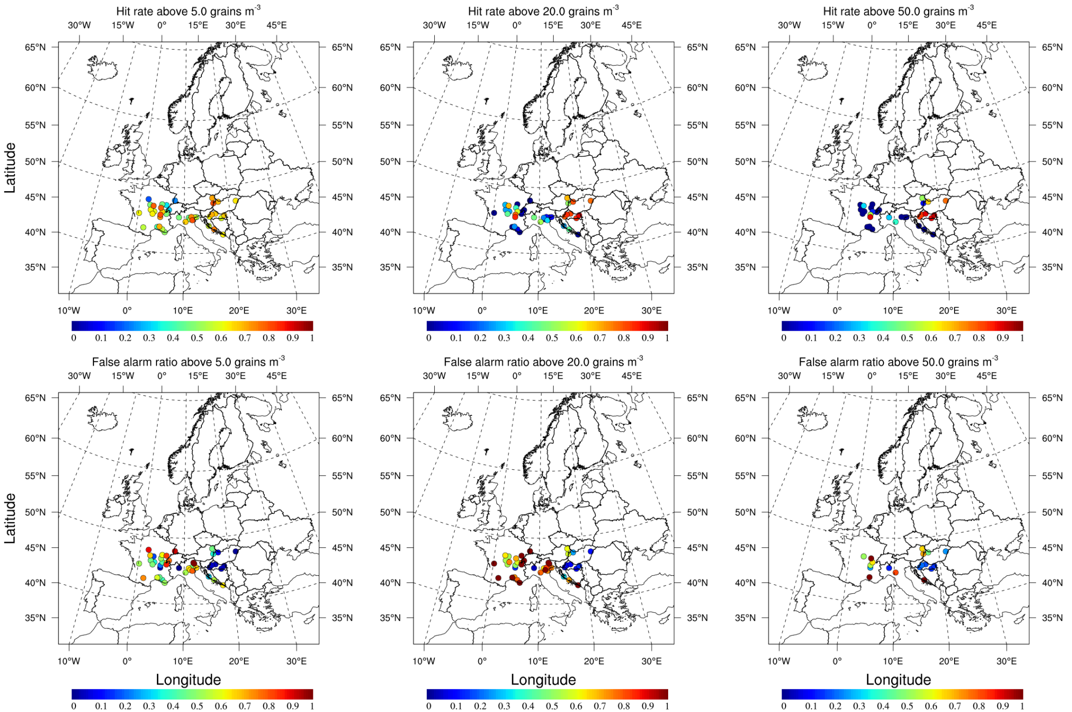

Figure 11. Categorical statistics at thresholds of 5 grains m^{-3} (left column), 20 grains m^{-3} (middle column), and 50 grains m^{-3} (right column): upper panel – hit rate (percentage of correctly predicted exceedances to all actual exceedances), lower panel – false alarm ratio (percentage of incorrectly predicted exceedances to all predicted exceedances).

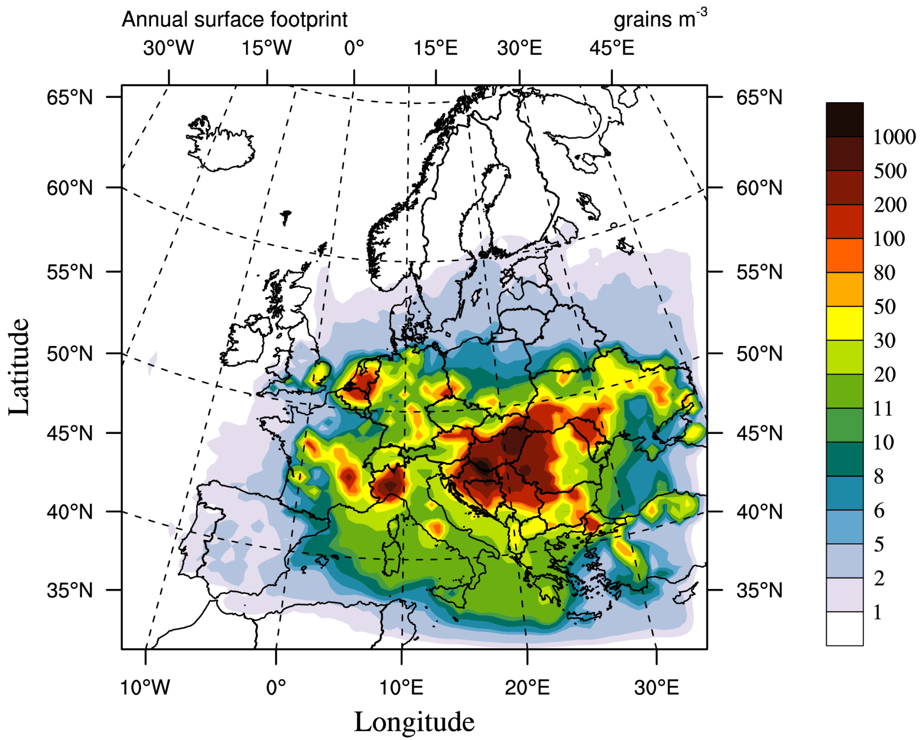

Figure 12. Annual footprint of ragweed pollen at the surface, obtained by selecting the maximum from daily averaged concentrations during the whole pollen season.

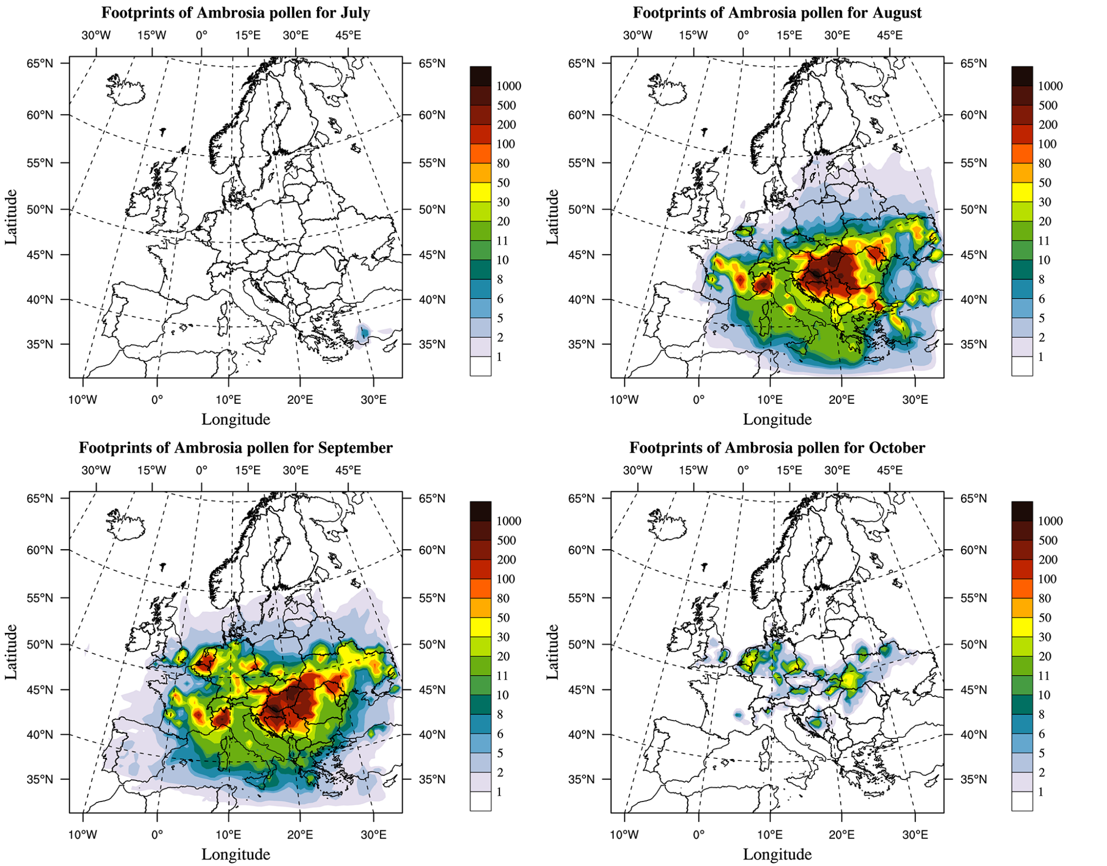

Figure 13. Footprints of ragweed pollen at the surface in each month during pollen season, average from 2000 to 2010, obtained by selecting the maximum from daily averaged concentrations in each month.

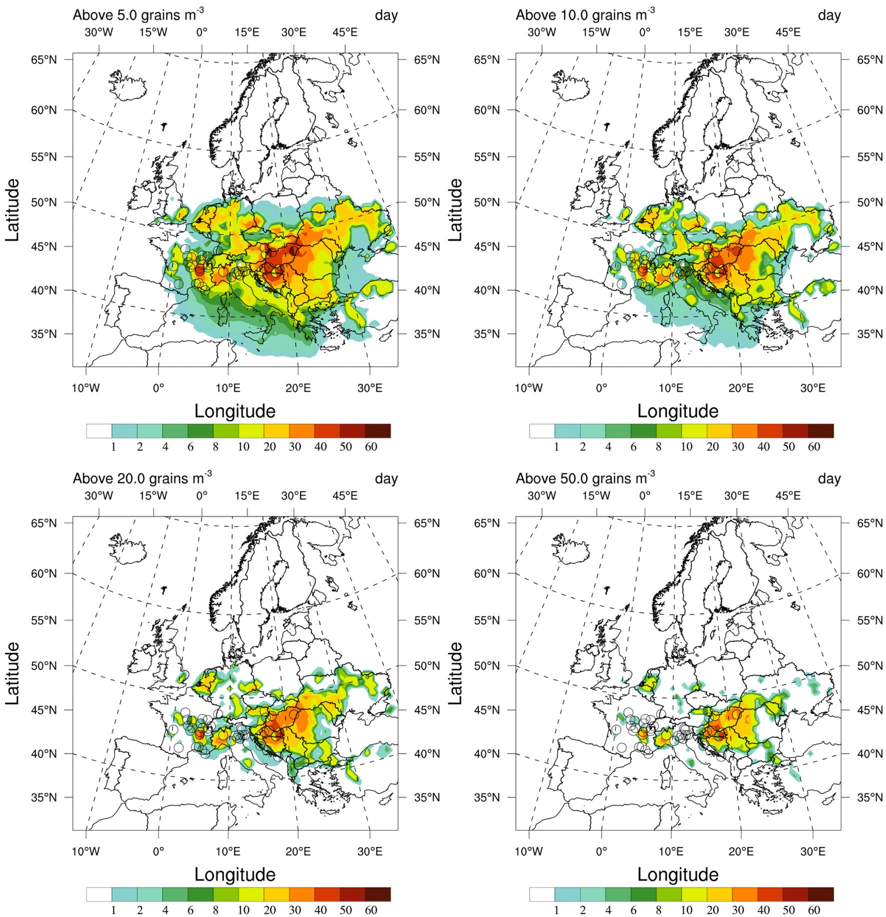

Figure 14. Number of days when the daily average concentration exceeding certain risk levels. Ground-based measurement locations are indicated with circles coloured by the measured number of days (left half) and corresponding simulated number of days (right half).

BGD
12, 17595–17641, 2015